Monitoring seismic damage via Accelerometer data alone using Volterra series and genetic algorithm.

NA Alexander[1], M Dietz[2], MM Kashani[3]

[1]Associate Professor, Department of Civil Engineering, University of Bristol

[2]Research Fellow, Department of Civil Engineering, University of Bristol

[3]Associate Professor, University of Southampton

Abstract

An application of Volterra series in nonlinear system identification is presented in this paper. This novel approach makes use of accelerometer data alone. The aim is to develop an algorithm that can rapidly detect damage, caused by earthquakes, in infrastructural systems without the need for a parallel transducer system that also monitors relative displacements around predicted damage locations. In addition, this algorithm (here termed Method A 'Acceleration only') is shown to be effective for low to high levels of damage. It first extracts the estimated multimodal linear kernel using a genetic algorithm applied to the input/output structural acceleration time-series. This enables a very precise estimate of linear system parameters. It then subsequently extracts quadratic and cubic nonlinear (kernel) terms by making use of multinomial combinations of the wavelet basis of the input signal. Extracted nonlinear kernel acceleration time-series and their standardised cumulative norms are compared with normalised hysteretic dissipated energy which requires both response accelerations and displacements, (here termed method A/D "Accelerations and displacements'). As a heuristic case we investigate the performance of both method A, and method A/D in predicting probable damage in a Bouc-Wen nonlinear system. Results suggest that method A/D and method A are comparable at estimating the likely maximum system ductility. We develop a fragility curve for estimating the probability of damage based on our nonlinear Volterra series intensity measure. Finally, we verify the application of this Volterra series approach against experimental test data from physical laboratory shake-table experiments of reinforced concrete columns and demonstrate that this approach is useable in practice.

1. Introduction

The current performance-based bridge design approach allows plastic hinges occurring in bridge piers to dissipate energy (Caltrans, 2013; CEN.EN, 2010). Therefore, the structural capacity and nonlinear dynamic behaviour of a bridge depends mainly on its piers. The nonlinear structural behaviour of reinforced concrete (RC) bridge piers is hugely affected by concrete cover spalling (Dhakal & Maekawa, 2002; Lehman et al., 2004), core concrete crushing (Lehman et al., 2004; Sheikh & Khoury, Tobbi et al., 2014), reinforcement yielding/fracture in tension (Kashani et al., 2018; Kim et al., 2005; Lehman et al., 2004), rebar buckling in compression (Dhakal & Maekawa, 2002; Kashani et al., 2018; Lehman et al., 2004), low-cycle fatigue degradation (El-Bahy et al., 1999; Kashani et al., 2018;), and corrosion damage (very common in most ageing bridges) (Alipour et al., 2011; Choe et al., 2008; Dizaj et al., 2018, 2020; Ghosh & Padgett, 2010; Kashani, Maddocks, et al., 2019). After any major natural disaster (e.g. earthquakes, floods etc.), assessment of the structural integrity of bridges is vital. Bridges, which cross natural barriers, are a very important source of vulnerability within transport networks. Bridge closure often results in significantly reduced traffic flows, and hence, interruption in rapid post-disaster rescue response. Therefore, it is crucial for bridge owners and managers to rapidly have an estimate of the extent of damage in major bridges. Moreover, the management, of state-owned, bridges and other civil infrastructural artefacts requires prioritisation of limited human resources to achieve rapid early interventions and plan appropriate medium term post-disaster recovery proposals. In conventional structural health monitoring and system identification, force and displacement responses, along with visual inspections, are required for estimating the damage in a structure following an earthquake. Inertial forces can be estimated by recording accelerations using accelerometers and calculating modal masses which requires in-situ ambient testing. However, it is almost impossible to measure the displacement time-series of a bridge (or a bridge pier) during an earthquake. For instance, Global Positioning System (GPS) generally does not have the necessary spatiotemporal resolution to be presently useful (Kijewski-Correa, 2005). Other technologies, such as measuring local deformations (optical/strain), are quite expensive (Ahlborn et al., 2010). Therefore, a novel approach that can rapidly evaluate the extent of damage in bridges using acceleration response alone is needed to help identify critically damaged bridges.

Thus, the fundamental question is what physical information do we need to achieve this high-level goal? A common practice in the earthquake engineering community is to use stiffness degradation under dynamic seismic loading to evaluate the structural damage (El-Bahy et al., 1999; Kim et al., 2005). However, quantification of stiffness degradation in damaged structures requires force and displacement response data. As discussed above, in-situ measurement of both force and displacement responses may not be practical. Alternatively, using impulsive loading the system transfer functions can be estimated before and after damage to determine any reduction in natural frequencies. While this can be estimated

using acceleration response time-series alone the resonant peak accuracy is limited by the duration of the free decay oscillations.

The proliferation of MEMs based accelerometers, Lynch JP et al (2007), Bhattacharya S. et. al. (2012), Ceylan H et al (2013), Galluci L et al. (2017), Bedon C et al (2018), coupled with mobile wireless technologies has resulted in the possibility of wide-scale low-cost monitoring of structural systems. It is now possible to actively monitor a whole class of state-wide vital infrastructural artefacts, such as bridges, hospitals, pipelines etc. The economic case for such an endeavour would be to identify and prioritise which artefacts require the most urgent visual inspection and intervention in the event of a large earthquake. Rapid post-earthquake assessment, Rainieri, C et al (2012), German S et al (2012), Goulet JA et al (2015), Cremen G et al (2018), is vital to ensure life-safety and for reducing the duration of the recovery phase.

However, while this concept seems very appealing, it does pose the question: is the data obtained from accelerometers sufficient to determine an estimate of damage? Ge et al, (2020a, b) has discussed and reviewed some of the existing algorithms in the literature that use time-frequency analyses for nonlinear structural system identification. They also developed a new method for rapid assessment of corrosion damaged RC bridges using time-frequency analysis techniques. In Ge et al, (2020a, b) 'Acceleration only' methods using standard transfer function estimates using Welch's method, the Hilbert transform, and Pseudo Wigner-Ville transform approaches are explored. These methods can identify the change in response frequencies with time that is an approximate match for a moving (in time) linear regression of stiffness which is based on 'Acceleration and Displacement' data. While these approaches offer some utility, experimental results indicate that they are most effective at very high levels of damage. It would be preferable to employ a method that functions over a broader range, i.e. low to high levels of damage. This would provide the greatest scope in setting a damage threshold level for visual inspection in a rapid post-earthquake assessment scenario.

Measurements of structural displacements are ideally needed to calculate the total energy dissipated in a nonlinear ductile hysteretic loop. Ideally, these relative displacements must be measured across zones of localised plasticity, which assumes we have a fairly good idea where the damage is located. As an alternative, one might attempt the double integration of response accelerations to produce response displacements. This procedure is, however, fraught with the difficulty of the amplification of low-frequency noise in the acceleration signal, Chanerley et al (2009, 2013). The typical amelioration to this problem is to low-cut filter the acceleration signals. This approach is reasonable for the case of an elastic system where there is no permanent deformation. However, for a nonlinear ductile system this low-cut filtering gives completely the wrong estimates of deformation.

It is, of course, possible to measure structural displacements using an independent transducer system. GPS, while a relatively mature technology, does not have the spatial or temporal resolution at present to measure very small deflections at a high sampling rate. Laser displacement transducers, Giri, P et al (2016), Giri, P et al (2017), Vicente MA et al (2018) can be used but these will require a greater cost than relying on just accelerometers alone.

Conceptually, infrastructure owners will have a choice between a range of options spanning (i) monitoring a larger number of structural systems with minimal instrumentation in the form of low-cost accelerometers (method A, 'record accelerations only') or (ii) monitoring far fewer structures using a multi-sensor platform of acceleration and displacement transducers (method A/D, 'record accelerations & displacements'). A rational decision, from within these options, must be grounded on the expected utility of each option. In the presence of very large damage Ge et al, (2020a, b) suggested that there is utility in method A and applying various time-frequency analyses of the acceleration data recorded. However, for the case of low to moderate damage, where only a "small" system nonlinearity is present, the acceleration only methods used in Ge et al, (2020a, b) appear to be far less effective at accurately characterising the extent of damage.

In this paper, we explore the expected utility of method A in combination with an application of Volterra series to this inverse system identification problem. Volterra series have been shown to be useful for a wide range of nonlinear systems. A good review of the various approaches in Volterra series identification is given in Libera et al (2021). The problem of dimensionality, that is the factorial growth in the number of multinomial terms with the adopted polynomial degree leads to computational complexity. A range of different strategies have been proposed in the literature, such as forward orthogonal least squares (Billings et al (1989)), variance analysis (Lind and Ljung (2005)), kernel-based regularization (Schölkopf & Smola, (2001)), a time-delay neural network (De Paula et al (2020)) etc

The question posed by this paper is this: can the level of seismically induced damage in a structure be determined from acceleration data alone? For large and complex structures, it is probably expedient to mount many accelerometers as it may not be obvious, a-priori, where damage is likely situated. However, for the case of bridges where critical components are known, i.e. the bridge piers, then only a pair of accelerometers per pier (one at the base and one at the top of a bridge pier) might be sufficient for monitoring damage of this component. Therefore, in this paper, we seek to characterise a simple nonlinear system that is defined by a single input and a single output. Generalisation to the nonlinear multi-input-multi-output (MIMO) case is beyond the present scope. In this paper we are investigating an application of Volterra series to predict levels of structural damage in critical components. We aim for a method that is reasonably accurate for low to medium levels of damage.

2.0 Detecting the fingerprint of nonlinearity from a system's responses.

2.1 A Volterra series, input-output, nonlinear system representation.

A Volterra Series, dating back to Volterra (1887), and its more recent discrete, digital, formulations, Schetzen, M. (1980), Rugh W.J. (1981), Fa-Long, L. (2011), Alexander et al, (2014), can be used to define some arbitrary nonlinear transformation of a signal $s_0(t)$ (an input) into a different signal $s_1(t)$ (an output). Characterising this transformation explicitly will enable us to determine the extent of nonlinearity in the signal $s_1(t)$ with respect to signal $s_0(t)$. In this paper, let $s_0(t)$ be the recorded ground motion $\ddot{x}_g(t)$ and let $s_1(t)$ be the recorded total acceleration response, at some point on the structure, (which includes any damage effects due to nonlinearity) to the given recorded event $\ddot{x}_g(t)$. Thus, we are seeking to characterise the abstract and unknown nonlinear transformation of the recorded ground motion $\ddot{x}_g(t)$ into the nonlinear total acceleration responses $s_1(t)$. Note, both $s_0(t)$ and $s_1(t)$ only require accelerometers (method A). We make no use of deformation data (between the top and bottom of the structure).

A Volterra series can capture, to some extent, multiple-scale delay effects caused by nonlinear hysteretic processes. Thus, the response signal $s_1(t)$ can be dependent on the input signal $s_0(t-t_i)$ at some time t_i delay. A general form of a Volterra series, in the time domain, involves the summing of multiple weighted convolution integrals of the input signal s_0.

$$\begin{aligned} s_1(t) &= \kappa_1(t) + \kappa_2(t) + \kappa_3(t) + \cdots \\ &= \int h_1(t_1) s_0(t-t_1)\,\mathrm{d}t_1 + \int\int h_2(t_1,t_2) s_0(t-t_1) s_0(t-t_2)\,\mathrm{d}t_1\,\mathrm{d}t_2 \cdots \\ &\quad + \int\int\int h_3(t_1,t_2,t_3) s_0(t-t_1) s_0(t-t_2) s_0(t-t_3)\,\mathrm{d}t_1\,\mathrm{d}t_2\,\mathrm{d}t_3 + \cdots \end{aligned} \tag{1}$$

The convolution integrals above permit multiple delays (phase lags) between input and output to be captured in the model. The weighting functions $h_n(t_1,\cdots,t_n)$ scale the amplitude for these delayed signals. By taking the Fourier transform of Eq (1) and re-expressing, which is by no means a simple matter, it can be demonstrated [Schetzen, M. (1980), Rugh W.J. (1981), Powers et al, (1989), Lang and Billings (1997), Tawfiq and Vinh (2004)], that Eq (1) is transformed into the frequency domain as follows,

$$S_1(\omega) = \kappa_1(\omega) + \kappa_2(\omega) + \kappa_3(\omega) + \cdots \tag{2}$$

where the linear Volterra terms κ_1 are defined as follows

$$\kappa_1(\omega) = H_1(\omega) S_0(\omega) \tag{3}$$

And the quadratic terms are expressed in terms of an associative function, defined as follows

$$\kappa_{(2)}(\omega_1,\omega_2) = H_2(\omega_1,\omega_2) S_0(\omega_1) S_0(\omega_2) \tag{4}$$

its 2-dimensional inverse Fourier transform as follows

$$\kappa_2(t) = \kappa_2(t,t) = \frac{1}{(2\pi)^2} \iint \kappa_{(2)}(\omega_1,\omega_2) e^{i(\omega_1+\omega_2)t} \mathrm{d}\omega_1 \, \mathrm{d}\omega_2 \tag{5}$$

Similarly, the cubic are defined in terms of an associative function

$$\kappa_{(3)}(\omega_1,\omega_2,\omega_1) = H_2(\omega_1,\omega_2,\omega_3) S_0(\omega_1) S_0(\omega_2) S_0(\omega_3) \tag{6}$$

And its 3-dimensional inverse transform is defined as follows

$$\kappa_3(t) = \kappa_3(t,t,t) = \frac{1}{(2\pi)^3} \iiint \kappa_{(3)}(\omega_1,\omega_2,\omega_3) e^{i(\omega_1+\omega_2+\omega_3)t} \mathrm{d}\omega_1 \, \mathrm{d}\omega_2 \, \mathrm{d}\omega_3 \tag{7}$$

2.2 Extract linear kernel

The problem with practically employing this Volterra series equation (3) is in obtaining a reasonably accurate mathematical description of the kernels $H_i(\omega)$. We know the definition of the linear kernel $H_1(\omega)$ from known dynamics theory but the nonlinear kernels $H_2(\omega_1,\omega_2), H_3(\omega_1,\omega_2,\omega_3)$ etc are dependent on the nature of the system's nonlinearity and therefore uncertain. The linear kernel $H_1(\omega)$ can be obtained from the solution of the linear differential equations of the structural system under analysis. For example, for a *m*-dof/mode idealisation, the linear kernel takes the form as follows,

$$\delta S_1(\omega) = H_1(\omega : \gamma_1, \omega_1, \alpha_1, \beta_1, \cdots) \delta S_0(\omega) \tag{8}$$

where $\delta S_0(\omega)$ is the small amplitude frequency domain representation of a recorded ground motion acceleration and $\delta S_1(\omega)$ is the small amplitude total acceleration response (of a system dof), for the system under consideration. Here, the term 'small amplitude' implies sufficiently small so that only linear responses are discernible. The linear kernel is defined as follows:

$$H_1(\omega : \gamma_1, \omega_1, \alpha_1, \beta_1, \cdots) = \sum_{i=1}^{m} \frac{\rho_{i1} + \mathbf{i}\omega\rho_{i2}}{\omega_i^2 - \omega^2 + \mathbf{i}2\gamma_i\omega_i\omega} \tag{9}$$

where H_1 is a frequency dependant function of 4*m* unknown system parameters, namely, the ratios of critical damping γ_i, linear natural circular frequencies ω_i and participation parameters ρ_{i1}, ρ_{i2}. These participation parameters depend on the mode shape's coordinates at the dof under consideration and systems damping and stiffness models. The derivation of equation (9) is described in Appendix A.

We make use of this multi-modal parametric form, equation (9), to fit experimentally obtained low-amplitude ambient vibration data. This benefits from (i) using all acceleration times-series data points,

rather than just peaks as in the classical methods of logarithmic decrement, half-power bandwidth etc, and (ii) it also accommodates multi-modal responses which are very typical in practice rather than making use of a single mode idealisation. This later point (ii) is critical if accurate extraction of the linear kernel is to be achieved. Thus, we seek an inverse linear system identification by constructing the following nonlinear optimisation problem to determine these 4*m* unknown parameters,

$$\min_{\gamma_1,\omega_1,,\alpha_1,\beta_1,\cdots} \frac{\int\left(\delta S_1 - H_1\left(\omega:\gamma_1,\omega_1,\rho_{11},\rho_{12},\cdots\right)\delta S_0\right)^2 \mathrm{d}\omega}{\int \delta S_1{}^2 \mathrm{d}\omega} \tag{10}$$

A genetic algorithm (Goldberg (1989), Conn AR et al, (1991, 1997)) is ideally suited to this problem as it doesn't require an initial guess for the damping ratios γ_i natural frequencies ω_i or participation parameters ρ_{i1},ρ_{i2}. It also seeks a global optimum, rather than some local optima typical of more traditional nonlinear optimiser such as the interior point algorithm (Byrd et al, (1999,2000)). Having said this, we make use of a hybrid approach where the genetic algorithm (which is better suited to searching the parameter space) identifies the probable location of the global minimum. It then hands this solution over to the interior point algorithm for final faster convergence to achieve a higher precision estimate of this global minimum. Ideally, in this problem, the structural system should be behaving linearly. Therefore, we need recordings from some low-amplitude ground-borne vibration (input) $\delta S_0(\omega)$ (a small earthquake) and its twin total acceleration response (output) $\delta S_1(\omega)$. This should ensure that the structural system is behaving linearly. In the experimental shake-table test results (section 5) we shall make use of low-amplitude white noise tests. Under these conditions, implementation of the genetic algorithm (hybrid option) is straightforward, and it enables very precise estimates of the linear structural parameters.

Now we are able to estimate the linear term κ_1 for any earthquake S_0 using the known linear kernel form (8) and the optimally estimated system parameters $\gamma_1,\omega_1,\rho_{11},\rho_{12},\cdots$, hence

$$\kappa_1 = H_1\left(\omega:\gamma_1,\omega_1,\rho_{i1},\rho_{i2},\cdots\right)S_0 \tag{11}$$

Once we obtain an estimate of the linear kernel, equation (3) can be expressed as follows.

$$S_2(\omega) = S_1(\omega) - \kappa_1(\omega) = \kappa_2(\omega) + \kappa_3(\omega) + \cdots \tag{12}$$

where S_1 is the total acceleration system response (due to linearity and nonlinearity), κ_1 is the component of the response acceleration due to linearity, and S_2 are the components of the structural response due to nonlinearity.

2.3 Using stationary wavelet transform to approximate the nonlinear terms.

To discretise the expression (12) we first express the input signal $s_0(t)$ as a sum of narrow frequency sub-band components $\varphi_i(t)$ as follows,

$$s_0(t) = \sum_{i=1}^{m} \varphi_i(t), \quad m \ll n \tag{13}$$

A wavelet decomposition (using the stationary wavelet decomposition, see Nason and Silverman (1995), Coifman and Donoho (1995), Pesquet et al (1996)), as in Alexander et al (2014), can be adopted where $\varphi_i(t)$ is the *i*th wavelet decomposition level of $s_0(t)$. In this paper we make use of the biorthogonal mother wavelet 'bior1.1'. This wavelet is employed because it has a very small number of filter coefficients, and hence each wavelet level sub-band spans the smallest range of frequencies. For earthquake signals, which are duration limited, the number of wavelet sub-bands, with 'bior1.1' is typically between 11 and 14. Therefore, the subsequent assumption that each wavelet level is a narrow-band process is more correct than if we use wavelets with larger numbers of coefficients such as 'bior6.8'. It is also worth noting that results are similar if one uses Daubechies mother wavelet 'db1'. The frequency domain version of equation (13) is obtained by the Fourier integral transform. Thus $S_0(\omega) = \mathcal{F}\{s_0(t)\}$ and $\phi_i(\omega) = \mathcal{F}\{\varphi_i(t)\}$ where $\mathcal{F}\{\ \}$ is Fourier integral transform of a signal. In this paper we use the FFT algorithm for determining the discrete version of $\mathcal{F}\{\ \}$. Hence by substituting, the frequency domain version of equation (13) into (12) we obtain the following approximation

$$\kappa_{(2)}(\omega_1,\omega_2) = \sum_{i=1}^{m}\sum_{j=1}^{m} H_{ij}\phi_i(\omega_1)\phi_j(\omega_2) \tag{14}$$

$$\kappa_{(3)}(\omega_1,\omega_2,\omega_3) = \sum_{i=1}^{m}\sum_{j=i}^{m}\sum_{k=j}^{m} H_{ijk}\phi_i(\omega_1)\phi_j(\omega_2)\phi_k(\omega_3) \tag{15}$$

where H_{ij} are coefficients that approximate the second kernel $H_2(\omega_1,\omega_1)$ and H_{ijk} are coefficients that approximate the third kernel $H_3(\omega_1,\omega_2,\omega_3)$. We assume that since the wavelet levels are narrow band processes that we can approximate the nonlinear kernels by a set of coefficients. Cheng et al (2015) uses and analogous procedure that uses a wavelet balance method to derive sub-band Volterra series outputs in the time-domain.

Because the associative function $\kappa_{(2)}(\omega_1,\omega_1)$ is the product of two independent functions $\phi_i(\omega_1)$ and $\phi_j(\omega_1)$ then equation (5) can be simplified by making use of the separability property, thus

$$\begin{aligned}\kappa_2(t) &= \sum_{i=1}^{m}\sum_{j=i}^{m}\frac{1}{(2\pi)^2}\iint H_{ij}\phi_i(\omega_1)\phi_j(\omega_2)e^{i(\omega_1+\omega_2)t}\,\mathrm{d}\omega_1\,\mathrm{d}\omega_2 \\ &= \sum_{i=1}^{m}\sum_{j=i}^{m}H_{ij}\frac{1}{(2\pi)}\int\phi_i(\omega_1)e^{i(\omega_1)t}\,\mathrm{d}\omega_1\,\frac{1}{(2\pi)}\int\phi_j(\omega_2)e^{i(\omega_2)t}\mathrm{d}\omega_2 \\ &= \sum_{i=1}^{m}\sum_{j=i}^{m}H_{ij}\phi_i(t)\phi_j(t)\end{aligned} \tag{16}$$

where $\phi_i(t)$ is the inverse Fourier transform of $\phi_i(\omega_1)$ and $\phi_j(t)$ is the inverse Fourier transform of $\phi_j(\omega_2)$. And similarly, the third kernel can be expressed as follows

$$\kappa_3(t) = \sum_{i=1}^{m}\sum_{j=i}^{m}\sum_{k=j}^{m}H_{ijk}\phi_i(t)\phi_j(t)\phi_k(t) \tag{17}$$

Now it is possible to use equations (16) and (17) in the time domain. However, in this paper we use an analogous set of equations in the frequency domain and note that these are not identical to the time domain equations (16) and (17) .

$$S_2(\omega) = \underbrace{\sum_{i=1}^{m}\sum_{j=i}^{m}H_{ij}\phi_i\phi_j}_{\text{Quadratic terms}} + \underbrace{\sum_{i=1}^{m}\sum_{j=i}^{m}\sum_{k=j}^{m}H_{ijk}\phi_i\phi_j\phi_k}_{\text{Cubic terms}} + \cdots \tag{18}$$

The reason why we are using these analogous set of equations, which do not follow directly from (1) is that it performs better than the time-domain version equations (16) and (17). This frequency analogous set of equations (18) mitigates, to some extent, the convolution that is missing in the time-domain version that is due to the approximation of the kernels employed.

As one final adjustment we normalise the quadratic $\phi_i\phi_j$ and cubic $\phi_i\phi_j\phi_k$ wavelet combinations terms to re-scale the subsequent least squares process to improve its numerical stability.

Hence, eqn (15) becomes

$$S_2(\omega) = \underbrace{\sum_{i=1}^{m}\sum_{j=i}^{m}b_{ij}\psi_{ij}}_{\text{Quadratic terms}} + \underbrace{\sum_{i=1}^{m}\sum_{j=i}^{m}\sum_{k=j}^{m}b_{ijk}\psi_{ijk}}_{\text{Cubic terms}} + \cdots \tag{19}$$

where the normalised wavelet combinations are

$$\psi_{ij} = \frac{\phi_i\phi_j}{\|\phi_{ij}\|_2}, \quad \psi_{ijk} = \frac{\phi_i\phi_j\phi_k}{\|\phi_{ijk}\|_2} \tag{20}$$

and the Euclidean norms are defined as follows

$$\left\|\phi_{ij}\right\|_2 = \sqrt{\int \left(\phi_i \phi_j\right)^2 \mathrm{d}\omega}$$
$$\left\|\phi_{ijk}\right\|_2 = \sqrt{\int \left(\phi_i \phi_j \phi_k\right)^2 \mathrm{d}\omega} \tag{21}$$

And the scaled kernel coefficients are defined as follows

$$b_{ij} = H_{ij}\left\|\phi_{ij}\right\|_2, \quad b_{ijk} = H_{ijk}\left\|\phi_{ijk}\right\|_2 \tag{22}$$

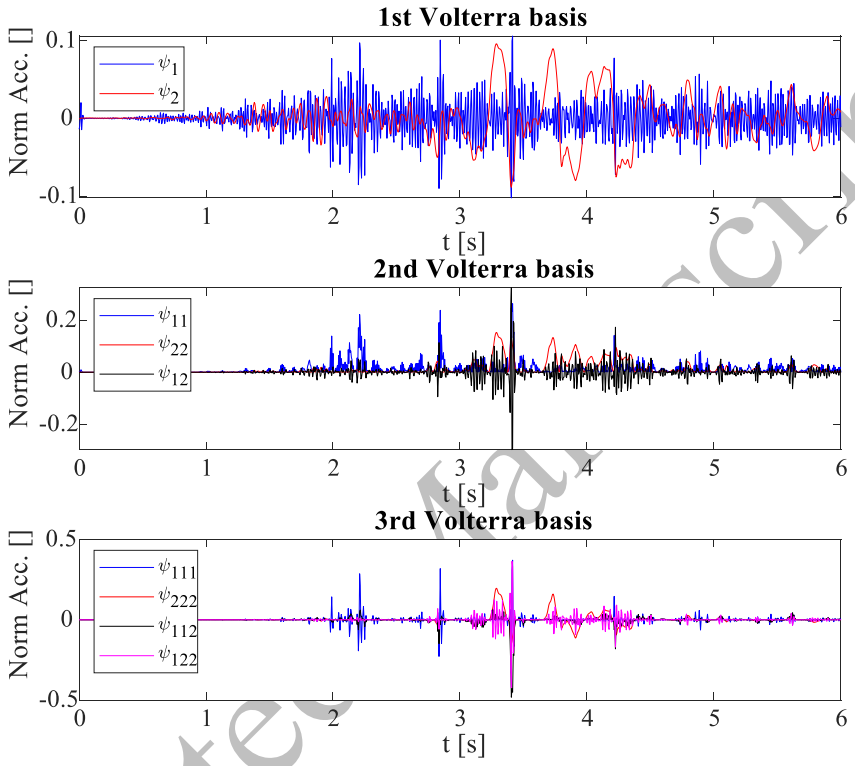

Figure 1, Example Volterra basis functions assuming two term wavelet decomposition for accelerogram Loma Prieta event 10/18/89, record NGA 765, PEER database

As an explanatory example, we display in **Figure 1** (in the time-domain) a two-term ($m=2$) wavelet decomposition of an recorded accelerogram from the PEER database which results in a 3 term basis for the quadratic Volterra terms and a 4 term basis for the cubic terms. Note that in practice, in this paper, we perform wavelet decomposition up to the maximum level permitted, which is typically $m>11$ terms (dependant on the length of the earthquake timeseries). The total number of coefficients in (19) is q defined as follows

$$q = \frac{(p+m)!}{p!m!} + (m-1) \tag{23}$$

where p is the number of Volterra kernels and m the number of wavelet levels used to decompose the input signal $\mathbf{s}_1$. As an example, ground motion 13 is a timeseries of 5996 points and a maximum wavelet decomposition of $m = 13$. Hence the total number of coefficients is 546.

2.4 Sequentially extracting the higher order terms

The discrete, vectorised, form, for the frequency domain representation of Volterra series equation (19) , that only includes nonlinear terms is as follows,

$$\mathbf{S}_2 = \underbrace{\left[\boldsymbol{\psi}_{11},\ldots,\boldsymbol{\psi}_{mm}\right]\mathbf{b}_2}_{\text{Quadratic terms}} + \underbrace{\left[\boldsymbol{\psi}_{111},\ldots,\boldsymbol{\psi}_{mmm}\right]\mathbf{b}_3}_{\text{Cubic terms}} + \cdots = \boldsymbol{\Psi}_2\mathbf{b}_2 + \boldsymbol{\Psi}_3\mathbf{b}_3 + \cdots, \tag{24}$$

First, let us consider the quadratic terms: each column matrix $\boldsymbol{\Psi}_2$ is a discrete form of ψ_{ij}. It represents one normalised quadratic combination of wavelet levels ϕ_i and ϕ_j. Similarly the cubic terms: each column matrix $\boldsymbol{\Psi}_3$ is a discrete form of ψ_{ijk} represents one normalised cubic combination of wavelet levels ϕ_i, ϕ_j and ϕ_k. These equations (24) are a set of complex linear algebraic equations in terms of complex weights, $\mathbf{b}_2, \mathbf{b}_3, \cdots$. It is possible to solve algebraic equations (24) in a least squares sense altogether (for a finite number of kernels). However, in practice, it is better to progressively extract each kernel separately. Therefore, we obtain the unknown quadratic weights by solving $\mathbf{S}_2 = \boldsymbol{\Psi}_2\mathbf{b}_2$ hence $\tilde{\mathbf{b}}_2 = \boldsymbol{\Psi}_2^{+}\mathbf{S}_2$ where Ψ_2^{+} is the pseudo inverse (Moore-Penrose) of Ψ_2. Hence, we can construct the quadratic terms

$$\boldsymbol{\kappa}_2 = \boldsymbol{\Psi}_2\boldsymbol{\Psi}_2^{+}\mathbf{S}_2 \tag{25}$$

And so we subtract out our estimate of the quadratic terms $\boldsymbol{\kappa}_2$ from equation (24) to leave us with the cubic and higher order terms, as follows

$$\mathbf{S}_2 - \boldsymbol{\kappa}_2 = \mathbf{S}_3 = \underbrace{\left[\boldsymbol{\psi}_{111},\ldots,\boldsymbol{\psi}_{mmm}\right]\mathbf{b}_3}_{\text{Cubic kernel terms}} + \cdots = \boldsymbol{\Psi}_3\mathbf{b}_3 + \cdots \tag{26}$$

And by a similar process

$$\boldsymbol{\kappa}_3 = \boldsymbol{\Psi}_3\boldsymbol{\Psi}_3^{+}\mathbf{S}_3 \tag{27}$$

Thus, we have an approach that effectively decomposes the response of a nonlinear system into linear, quadratic and cubic terms by using equations (11), (25) and (27) respectively. Finally, we can

reconstruct our estimate of the output signal $\tilde{\mathbf{S}}_1(\omega)$ (here the structure's total acceleration response) thus,

$$\tilde{\mathbf{S}}_1 = \sum_{i=1}^{p} \boldsymbol{\kappa}_i \tag{28}$$

In the examples shown in this paper, the correlation coefficient squared between the estimated (reconstructed) response $\tilde{\mathbf{S}}_1$ and the measured (actual) response $\mathbf{S}_1$ is typically $r^2 \approx 0.998$ using just three kernels. Therefore, we assume $\tilde{\mathbf{S}}_1 = \mathbf{S}_1$. It is worth noting that we ensure that the extracted $\boldsymbol{\kappa}_i$ must have even real parts and odd imaginary parts in order that $\mathcal{F}^{-1}\{\boldsymbol{\kappa}_i\}$ is real function, where $\mathcal{F}^{-1}\{\ \}$ is the inverse Fourier transform of a signal. This can be simply achieved by (i) assuming that equations (25), (27) and so on, apply only to positive frequencies below the Nyquist frequency ω_{nyq} and by (ii) reconstructing the negative frequency coefficients of $\boldsymbol{\kappa}_i$ by assigning them values that ensure real components exhibit evenness and imaginary components exhibit oddness.

2.5 Method A 'Acceleration only' damage measure

We conclude that if the first Volterra vector $\boldsymbol{\kappa}_1(t) \approx \mathbf{s}_1(t)$ then a simple linear system would capture the transformation from $s_0(t)$ to $s_1(t)$; and so the structure is behaving linear elastically. In this case the nonlinear vectors (quadratic $\boldsymbol{\kappa}_2$, cubic $\boldsymbol{\kappa}_3$ and so on) should have very small magnitudes. We define the cumulative magnitude of the ith term as $D_{i,j}$ at time $t = (j-1)/f_s$ where f_s is the sampling frequency in Hz. This $D_{i,j}$ is non-dimensional, by normalising it with respect to the magnitude of the ground motion; and is thus defined as follows,

$$D_{i,j} = \frac{\sqrt{\sum_{r=1}^{j} \kappa_{i,r}^2}}{\sqrt{\sum_{r=1}^{n} s_{0,r}^2}}, \qquad \boldsymbol{\kappa}_i(t) = \left[\kappa_{i,1}, \kappa_{i,2}, \cdots\right] \in {}^{\sim n\times 1}, \qquad \mathbf{s}_0(t) = \left[s_{0,1}, s_{0,2}, \cdots\right] \in {}^{\sim n\times 1} \tag{29}$$

where n is the total size of the ground motion vector $\mathbf{s}_0(t)$ and kernel series vectors $\boldsymbol{\kappa}_i(t)$. We shall employ $D_{i,j}$ (for nonlinear kernel series, $i > 1$) as a measure ('fingerprint') of damage with time, and $D_{i,n}$ (for nonlinear kernel series, $i > 1$) as a measure of total damage.

In the following sections we shall explore the performance of the algorithm describe in section 2 for (i) a numerical model that typically defines a nonlinear hysteretic system, namely a single dof Bouc-Wen idealisation and (ii) using recorded data from real column tests performed in the shake table Laboratory at the University of Bristol, Ge et al. (2020a, b, c).

3. Volterra/Genetic Algorithm method on Bouc-wen model output

3.1 Bouc-Wen model description

As a test case, consider a nonlinear single degree of freedom system with a general hysteretic nonlinearity of the Bouc-Wen type, Charalampakis A et al (2006), Song et al. (2006), Meibodi and Alexander (2020). The equation of motion is as follows,

$$\ddot{x}(t)+2\gamma_1\omega_1\dot{x}(t)+F\left(x(t)\right)=-\ddot{x}_{\mathrm{g}}(t), \qquad F\left(x(t)\right)=\omega_1^2 x_y \Omega\left(x(t),z(t)\right) \tag{30}$$

For the case of the columns in the later section of this paper, $x(t)$ would be located at the lumped mass at the column head and is the relative displacement with respect to the moving ground support. Therefore, Eq (30) is defined in terms of a moving coordinate frame which is typical in earthquake engineering. Note, the total acceleration $\ddot{x}_t$ of the lumped mass is $\ddot{x}+\ddot{x}_g$. The parameter γ_1 is the ratio of critical damping for a viscous (velocity proportional) damping model. The linear natural frequency is ω_1 which is defined for the undamaged, pristine, structure case. The nonlinear stiffness force per unit mass is $F\left(x(t)\right)$and will be described in detail by a generic hysterical Bouc-Wen model. This model is approximately linear and non-hysteretic up to a displacement $\left|x(t)\right|<x_y$ where the parameter x_y can be viewed as a yield displacement of the column. In practice however, the Bouc-Wen model and the physical Reinforced concrete columns do not have a clear and precise yield point. Therefore, this parameter should be viewed as a pseudo-yield point as it only approximately divides mechanical behaviour between elastic and inelastic. The forcing term on the right-hand side of the equation $\ddot{x}_{\mathrm{g}}(t)$ is a timeseries recording of the acceleration of the ground,

We introduce ductility $q(t)=x(t)/x_{\mathrm{y}}$ and equation (30) is re-expressed as

$$\ddot{q}(t)+2\gamma_1\omega_1\dot{q}(t)+\omega_1^2\Omega\left(q(t),z(t)\right)=-\frac{\ddot{x}_{\mathrm{g}}(t)}{x_{\mathrm{y}}} \tag{31}$$

The nonlinear (non-dimensional) 'stiffness' function Ω is defined as follows,

$$\Omega\left(q(t),z(t)\right)=\alpha q(t)+(1-\alpha)z(t) \tag{32}$$

where positive coefficient α acts in a dual manner simultaneously introducing nonlinear behaviour, when $\alpha<1$ and inducing a post-yield, "work hardening" type slope. By the introduction of the internal dof $z(t)$ (which is dimensionless) we can capture, phenomenologically, hysteretic behaviour with the following ancillary first order equation

$$\dot{z}(t)=\dot{q}(t)\left(\frac{1-\left(1+\xi_{\mathrm{k}}E(t)\right)\left(\beta\,\mathrm{sgn}\left(\dot{q}(t)z(t)\right)+(1-\beta)\right)\left|z(t)\right|^{N}}{1+\xi_{\mathrm{s}}E(t)}\right) \tag{33}$$

where β is a parameter that controls the size of the hysteretic loop (typically the range adopted is $0<\beta<1$), parameter N (where $N>0$) controls the yield corner sharpness of the transition from elastic to inelastic of the force/deflection curve, parameters $\xi_{\mathrm{s}},\xi_{\mathrm{k}}$ control the strength and stiffness degrading rates with respect to normalised dissipated energy E that is defined as follows,

$$E(t)=(1-\alpha)\int_0^t \dot{q}(t)z(t)\,\mathrm{d}t \tag{34}$$

It is worth considering the effect of the yield displacement x_{y} on the solution of this Bouc-wen system. The only effect of x_{y} in these equations (31) to (34) lies in the term ground motion excitation $\ddot{x}_{\mathrm{g}}(t)/x_{\mathrm{y}}$ in equation (31). Hence, we conclude that yield displacement inversely effects the effective ground motion amplitude, i.e. doubling the yield displacement is equivalent to halving the peak ground acceleration (PGA) of the ground motion. Thus, if we explore a range of ground motion amplitudes, we effectively also explore a range of yield displacements.

3.2 Method A/D 'acceleration & displacement' damage measure

We seek to compare the efficacy of method A 'Acceleration only' damage measure $D_{\mathrm{i,n}}$ (defined in equation (29) which makes use of the Volterra series expansion) with a method A/D 'acceleration and displacement' damage measure.

A standard approach, found in the literature Chopra (2019), takes equation (30) and integrates it with respect to relative displacement *x*. This makes use of acceleration, velocity and displacement measurements plus system parameter estimates of natural frequency ω_1 and damping ratio γ_1. Note for

method A/D the velocity time-series would have to be estimated by some composite filter of acceleration and displacement time-series, Noda et al (2016). Thus, following Chopra (2019), by integrating equation (30) with respect to relative displacement x (which is also the total deformation of the column) we obtain the work done (per unit mass) by all dissipative forces, and hence the following formulae are derived,

$$\int_0^x \left(\ddot{x}+\ddot{x}_{\mathrm{g}}\right)\mathrm{d}x+\int_0^x 2\gamma_1\omega_1\,\dot{x}\mathrm{d}x=-\int_0^x F\left(x\right)\mathrm{d}x \tag{35}$$

$$u_{\mathrm{I}}\left(t\right)=u_{\mathrm{R}}\left(t\right)+u_{\mathrm{G}}\left(t\right),\quad u_{\mathrm{R}}\left(t\right)=\int_0^x \ddot{x}\mathrm{d}x,\quad u_{\mathrm{G}}\left(t\right)=\int_0^x \ddot{x}_{\mathrm{g}}\mathrm{d}x, \tag{36}$$

$$u_{\mathrm{D}}\left(t\right)=\int_0^x 2\gamma_1\omega_1\,\dot{x}\mathrm{d}x,\quad u_{\mathrm{L}}\left(t\right)=\omega_1^2\int_0^x x\,\mathrm{d}\,x \tag{37}$$

Where $u_{\mathrm{I}}\left(t\right)$ is the work done (per unit mass) of inertia terms, $u_{\mathrm{D}}\left(t\right)$is the work done (per unit mass) of the linear viscous damping terms, and $u_{\mathrm{L}}\left(t\right)$is the work done (per unit mass) of the linear elastic stiffness terms. $u_{\mathrm{NL}}\left(t\right)$ is the work done (per unit mass) solely due to the nonlinear/hysteretic behaviour and is defined as follows:

$$u_{\mathrm{NL}}\left(t\right)=\int_0^x F\left(x\right)\mathrm{d}\,x-u_{\mathrm{L}}\left(t\right)=-u_{\mathrm{I}}\left(t\right)-u_{\mathrm{D}}\left(t\right)-u_{\mathrm{L}}\left(t\right) \tag{38}$$

This nonlinear work done $u_{\mathrm{NL}}\left(t\right)$can be evaluated directly from measurements of force per unit mass $F\left(x\right)$ for the case of a computational model (such as equations (31) to (34)). In the case of a physical experiment direct measurements of the nonlinear stiffness force are problematic. Therefore, by recording acceleration and displacement time-series, then computing velocity time-series (via a composite filter) and estimating system parameters ω_1 and γ_1 we can evaluate $u_{\mathrm{I}}\left(t\right)$, $u_{\mathrm{D}}\left(t\right)$ and $u_{\mathrm{L}}\left(t\right)$, and so determine $u_{\mathrm{NL}}\left(t\right)$. The integrals in equations (36) and (37) are evaluated using Green's theorem and the cumulative trapezium rule. This is preferred to employing a change of variable (as suggested in Chopra (2019)) that will introduce the relative velocity $\dot{x}\left(t\right)$ time-series inside these integrals. Note that for computational studies these alternative integration approaches produce exactly the same results. However, in the case of experimental data, it is more problematic to obtain accurate estimates of velocity time-series (via a composite filter or the explicit extra cost of mounting velocity transducers) and hence the integration approach using relative velocity $\dot{x}\left(t\right)$ time-series (with a change of variable) can lead to more noise in the solution than employing Green's theorem. In this paper the following method A/D damage measure is employed,

$$\Delta_j = \left| \frac{u_{\mathrm{NL},j}}{u_{G,n}} \right|, \qquad \mathbf{u}_{\mathrm{NL}} = \left[u_{\mathrm{NL},1}, u_{\mathrm{NL},2}, \cdots \right] \in {}^{\sim} {}^{n\times 1} \tag{39}$$

where $\mathbf{u}_{\mathrm{NL}}$ is the discrete vector form of $u_{\mathrm{NL}}(t)$, Δ_j at time $t = (j-1)/f_s$ where f_s is the sampling frequency in Hz. Damage measure Δ_j is the cumulative ratio of estimated nonlinear work done (per unit mass) normalised to the component of inertial work done by the ground acceleration alone $u_{\mathrm{G}}(t)$.

4 Application of Volterra Series to a Bouc-Wen type nonlinearity

4.1 A heuristic case of an idealised bridge pier

Consider a single degree of freedom (SDOF) idealisation of a bridge pier (with deck mass). It has an elastic period of 0.3s and a viscous damping ratio $\gamma = 0.05$. These values are in the range of benchmark experimental column shake table tests described in Kashani MM et al (2019), Ge X et al (2020a, b). The nonlinear structural system's response is characterised by a Bouc-Wen model. The yield corner sharpness $N = 2$ and post yield stiffness to linear stiffness ratio $\alpha = 0.05$. The hysteretic loop size parameter $\beta = 0.4$ and strength and stiffness degrading parameters are $\xi_{\mathrm{s}} = 0.3, \xi_{\mathrm{k}} = 0.15$ respectively. The yield displacement can be assigned by making use of empirical formulae described in Yashinsky et al, 2000, Aschheim, M., et al (1993). Priestley 2000, Meibodi AA et al 2020. Here we assume $x_{\mathrm{y}} = 0.01\mathrm{m}$. In this section we shall employ the strong earthquake ground motion time-series listed in Table 2, Appendix B.

4.2 Examples of Volterra time-series and their cumulative norms

Figure 2 shows the response of the nonlinear system to the scaled (with a PGA of 1m/s^2) ground motion 13. We extract the linear $\kappa_1(t)$, quadratic $\kappa_2(t)$ and cubic $\kappa_3(t)$ series, using the equations (11), (25) and (27) respectively. For this record and the 'bior1.1' mother wavelet the number of wavelet sub-bands *m* is 12. Figure 2 (Top panel) displays the time-history of these series. Given that the quadratic and cubic terms are visibly smaller than the linear series, we conclude from just the recorded acceleration time-series that the system behaves almost linearly elastically in this case. This can be more clearly observed, see Figure 2 (Bottom panel), from the normalised cumulative energy of the linear, quadratic, and cubic terms, namely $D_1(t)$, $D_2(t)$, $D_3(t)$ respectively (defined in equation (29), method A). In this figure we also add the normalised cumulative hysteretic energy $\Delta(t)$ (equation (39), method A/D) as a comparison. There appears to be a significant temporal correlation between $\Delta(t)$ and quadratic and cubic terms $D_3(t)$. We also display the normalised stiffness force – ductility loops in Figure 4(a) which highlight the linearity of the system responses for this case.

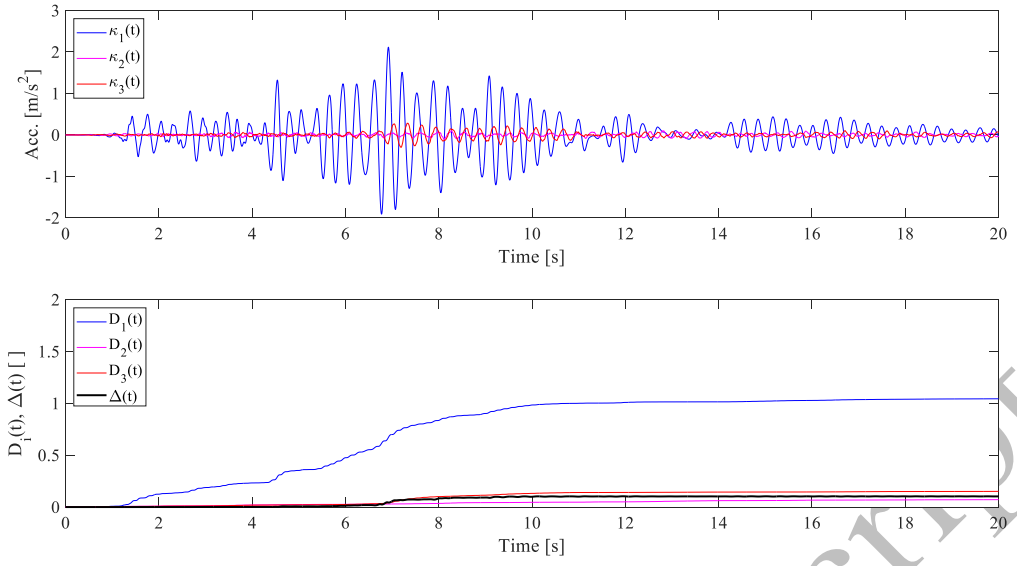

Figure 2, Ground motion Record 13 (PGA=1m/s^2)
(Top panel) Time-histories of linear $\kappa_1(t)$, quadratic, $\kappa_2(t)$ and cubic $\kappa_3(t)$ kernel series
(Bottom panel) Normalised cumulative energy of kernel series, linear $D_1(t)$, quadratic $D_2(t)$, cubic $D_3(t)$
(Method A) and normalised hysteretic damage measure $\Delta(t)$ (method A/D)

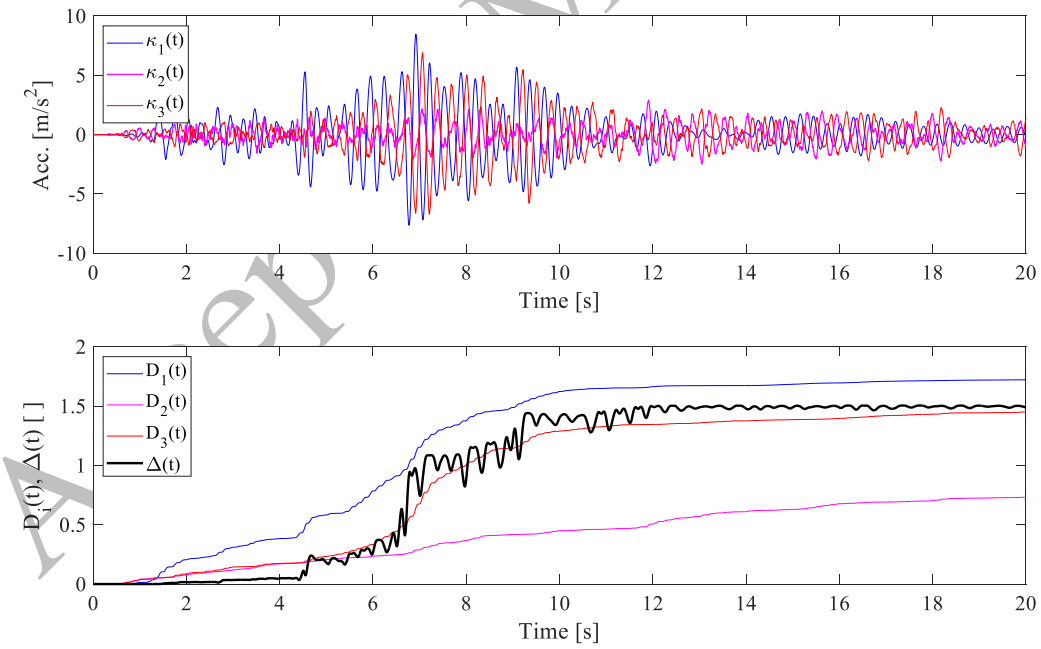

Figure 3, Ground motion Record 13 (PGA=4m/s^2)
(Top panel) Time-histories of linear $\kappa_1(t)$, quadratic, $\kappa_2(t)$ and cubic $\kappa_3(t)$ kernel series
(Bottom panel) Normalised cumulative energy of kernel series, linear $D_1(t)$, quadratic $D_2(t)$, cubic $D_3(t)$ and normalised hysteretic damage measure $\Delta(t)$

Figure 3 repeats this analysis case for a PGA of 4m/s^2. For this record and the 'bior1.1' mother wavelet the number of wavelet sub-bands *m* is 12. Here there has been a significant growth in the magnitude of

cubic kernel series $\kappa_3(t)$ and a smaller, but observable, growth in the quadratic $\kappa_2(t)$ kernel series. The match (temporally) between the normalised cumulative energy of the cubic kernel series $D_3(t)$ and normalised hysteretic energy $\Delta(t)$ is significant. Note also that the cubic series $\kappa_3(t)$ appears to be often in anti-phase with the linear kernel series $\kappa_1(t)$. For a linear system the total system response should increase proportionately with the amplitude of the forcing (i.e. the PGA). For the nonlinear system the total system response is the sum of all terms $\kappa_i(t)$ each of which commonly increases with the PGA. However, since the linear and cubic terms are often in anti-phase (as shown in fig 3(a)) the total system response may not increase significantly with increases in PGA for this system nonlinearity. This result is in keeping with what is expected in conventional capacity design which utilizes ductile structural behaviour. This structural ductility effectively acts as a mechanical "fuse" which serves to limit structural acceleration responses to some threshold level dictated by the structure's strength capacity. In this design philosophy, even though we do not know how large the next earthquake will be, we know the maximum acceleration and hence the maximum force on the structural system during this earthquake! The disadvantage of this approach is that ductile responses require plastic hinges and structural damage, so we trade structural damage for our lack of knowledge of the future earthquake's magnitude.

Figure 4 are force-deflection loops for the cases in Figure 2 and Figure 3. Note that these plots would, in practice, require the evaluation of the acceleration, velocity, displacement time-series and system parameter estimates. For this Figure 4, we have the numerical Bouc-Wen model which outputs both displacement and force. In a case of monitoring an actual structure in-situ with just accelerometers we would be unable to produce this plot. Figure 4(b) indicates serious nonlinear behaviour with a significant loss of stiffness during the earthquake as can be observed by considering the slope of the blue line (from 0-5s) and the black line (15-30s).

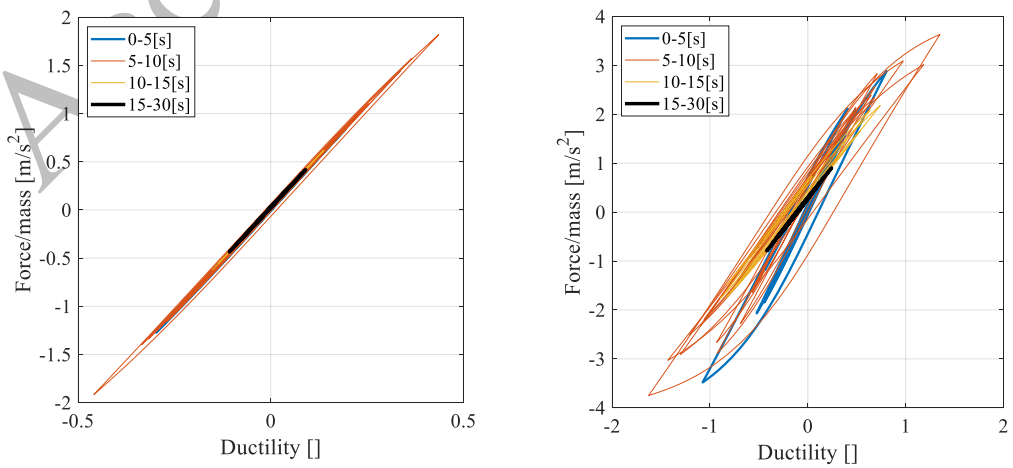

Figure 4, Normalised stiffness force - ductility hysteresis loops for Ground motion Record 13

(a) PGA 1m/s^2, (b) PGA=4m/s^2

4.3 Incremental dynamic analysis

Figure 5 are incremental dynamic analysis (IDA, Vamvatsikos, D., & Cornell, C. A. (2002)) plots. Figure 5(a) displays the final magnitude of linear, quadratic and cubic Volterra terms $D_{1,n}$ $D_{2,n}$ and $D_{3,n}$ respectively vs PGA for ground motion record 13. As expected, at low PGA the magnitude of the linear term $D_{1,n}$ is approximately 1 and quadratic and cubic magnitudes $D_{2,n}, D_{3,n}$ are approximately zero. This indicates linear elastic behaviour. Figure 4(b) displays the A/D damage measure vs PGA and Figure 4(c) displays the maximum ductility vs PGA. Hence Fig 4(c) could be viewed as the correct "damage measure" but it requires acceleration, velocity, displacement timeseries and all the parameters in the equation of motion, while Fig 4(b) represents the inferred damage using the work done formulation which requires acceleration and displacement timeseries and Fig 4(a) represents the inferred damage using only acceleration timeseries.

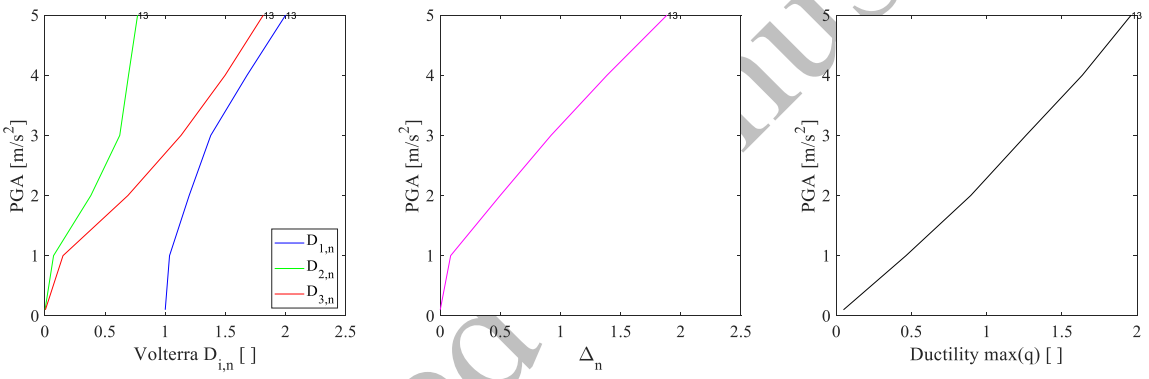

(a) (b) (c)

Figure 5, for ground motion record 13. The final magnitude of (a) Volterra magnitudes $D_{i,n}$ (method A) vs PGA. (b) normalised hysteretic damage Δ_n (method A/D) vs PGA (c) Maximum ductility vs PGA

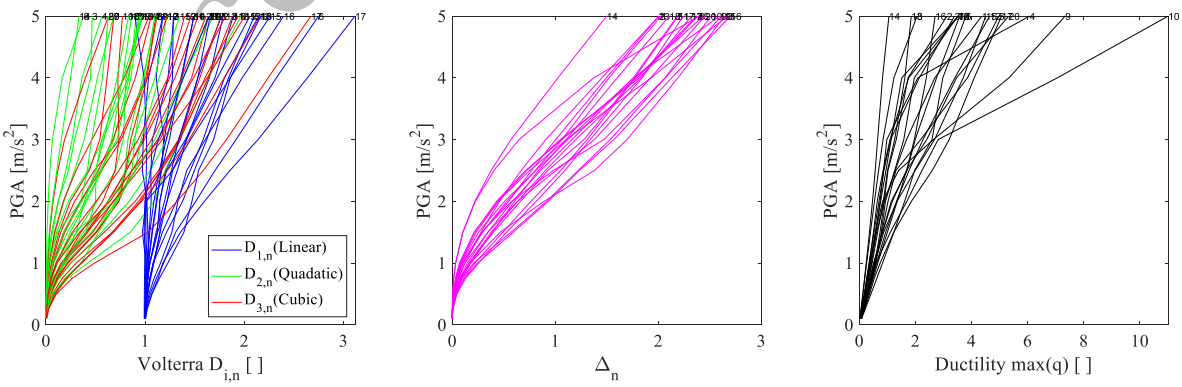

(a) (b) (c)

Figure 6, for all ground motions. The final magnitude of (a) Volterra magnitudes $D_{i,n}$ (method A) vs PGA. (b) normalised hysteretic damage Δ_n (method A/D) vs PGA (c) Maximum ductility vs PGA

Figure 6 extends the IDA analysis to all 20 ground motion records used in this paper and for a complete range of PGA from 0.1m/s^2 to 5m/s^2. The final magnitude of cubic terms $D_{3,n}$, (method A) is dependent, to some extent, on the ground motion time-series. This is also true of the damage measure Δ_n (method A/D) as shown in Figure 6(b). Each line in this figure is obtained from a different ground motion time-series. Figure 6(c) plots the maximum ductility vs PGA. For a physical experiment estimating ductility this would require both recording structural displacements and determining the yield displacement. Ductility may appear a preferable damage measure to Δ_n (which is hysteretic loop energy dissipation) as it has a clear interpretive quality. For example, if $\max(q)>1$ then we have likely inelastic action and damage. For the case of Δ_n it not clear what value of $\Delta_n > 0$ signifies the presence of actual inelastic behaviour in a general structural problem. However, estimating this ductility requires estimating the yield displacement which can be very problematic, Aschheim et al (1993). For the case of an undamaged (pristine) RC column the only way of determining the yield displacement is via (i) some empirical/theoretical formula, (ii) a numerical nonlinear pushover analysis or (iii) some destructive testing. Approaches (i) and (ii) can only estimate the yield displacement approximately while (iii) would damage the structure. Thus, ductility is much more difficult to estimate accurately for physical RC columns.

Results displayed in Figure 6(c) indicate that the Bouc-Wen model can, on occasion, produce very high values of system ductility. Note that Priestly et al. (1994) suggested that it is not common for the ductility of real physical RC columns to exceed 5. Thus, as our aim is to consider the nonlinear responses that might have some parallel for the case of the physical RC column artefacts. We shall assume all 'very high ductility' results are physically inadmissible outliers.

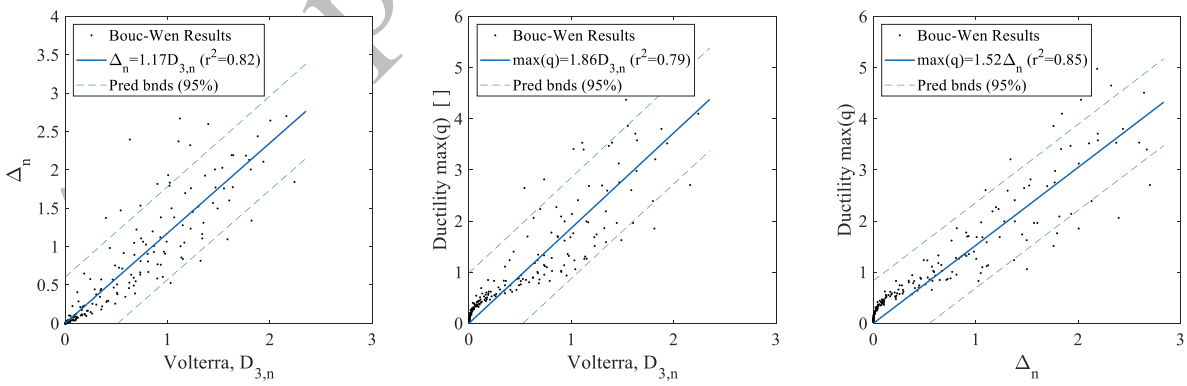

(a) (b) (c)

Figure 7, Bouc-Wen results (for ductility less than 5) for all ground motion records and PGA (0.1 to 5m/s^2)

(a) cubic Volterra $D_{3,n}$(method A) vs Damage measure Δ_n (method A/D) (b) cubic Volterra $D_{3,n}$(method A) vs max ductility $\max(q)$ (c) Damage measure Δ_n (method A/D) vs max ductility $\max(q)$

4.4 Statistical analysis of results and fragility curves

The correlation (across all ground motions and PGA values) between the cubic series damage measure $D_{3,n}$, (method A) and the damage measure Δ_n (method A/D) is displayed in Figure 7(a). Here the linear fitted function explains 82% of the observed variation in Δ_n. Similarly, the correlation between $D_{3,n}$ and the maximum ductility $\max(q)$ is displayed in Figure 7(b). Here the linear fitted function explains 79% of the observed variation in $\max(q)$. It is worth noting that the quadratic series damage measure $D_{2,n}$ explains 64% and 73% of the observed variation in Δ_n and $\max(q)$ respectively. Thus, the cubic appears to have a higher utility in predicting damage.

Remember that for this Bouc-Wen model obtaining an accurate damage estimate Δ_n is straight forward because all relevant response time-series and system parameters are known. For a general case of a physical RC column, it would require (i) measurements of acceleration and displacement (ii) re-construction via a composite filter of velocity time-series or introducing physical velocity transducers and (iii) using equations (35) to (39) (these equations assume a single dof idealisation) which requires accurate estimates of system parameters. Therefore, we observe that method (A/D) itself will require, at the very least, a determination of natural linear modal parameters, i.e. damping ratios and natural frequencies. If a standard log decrement, half power band width, power spectra approaches are adopted then these natural modal parameters cannot be determined very precisely. This parameter resolution problem can be alleviated by adopting the genetic algorithm multi-modal optimisation, equation (10) for both method A and method A/D. However, the secondary problem of using equations (35) to (39) is that it is based on a single dof idealisation. For the heuristic case in section 4, the nonlinear Bouc-Wen model is a single dof. Hence, for this case, we can ignore the uncertainties introduced in the damage measure Δ_n caused by a larger number of dofs. Consider the correlation between damage measure Δ_n (which is based on the area of the hysteretic loop) and $\max(q)$ shown in Figure 7(c). It appears that damage measure Δ_n (method A/D) is marginally better (85% as opposed to 79%) at predicting $\max(q)$ than $D_{3,n}$ (method A).

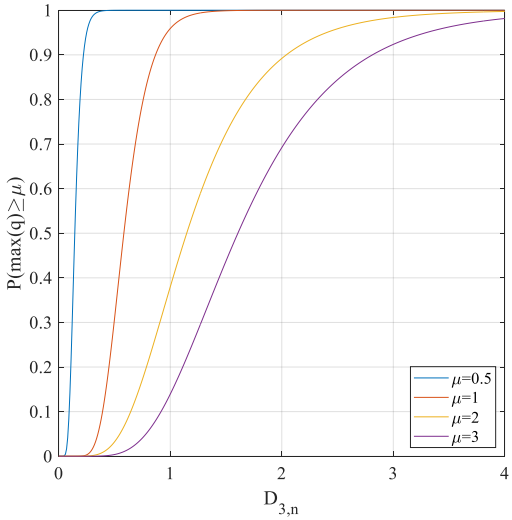

Figure 8, Using cubic term $D_{3,n}$ to predict the probability that ductility will exceed a certain threshold value (fragility curves)

Results in Figure 7 indicate a clear scatter in either predicting maximum ductility $\max(q)$ or hysteretic energy dissipation Δ_n using the cubic term $D_{3,n}$. Therefore we construct a cumulative probability graph (a fragility curve) which predicts for a given small interval of $0.9D_{3,n} \le D_{3,n} \le 1.1D_{3,n}$ what the probability $P(\max(q) > \mu)$ that the $\max(q)$ exceeds a given value μ . Figure 8 shows the fitted (statistically significant at 95% confidence level) cumulative lognormal distributions for various ductility thresholds μ. For example, consider a value of cubic term $D_{3,n} \approx 0.5$, this corresponds to a 30% probability that the maximum ductility is between 1 and 2. As another example, consider a value of cubic term $D_{3,n} \approx 1$, this corresponds to a 96% probability that the maximum ductility exceeds 1, a 37% probability that the maximum exceeds 2 and a 14% probability that the maximum ductility exceeds 3. Hence, if a given threshold ductility level is assigned along with a given acceptable probability level, then it is possible to assign a critical value of cubic term $D_{3,n}$ that would trigger a visual inspection of this structural system in a post-earthquake scenario.

5. Volterra/Genetic Algorithm method A on experimental RC column data

Laboratory experiments conducted at the University of Bristol; Ge et al. (2020a, b, c) were performed on a set of reinforced concrete columns. A series of white noise and large shake table tests were conducted with the measurement of response accelerations (using accelerometers) and displacements (using displacement transducers). White noise tests, that is broad-band ground vibrations at very low amplitude, were performed before and after every earthquake excitation to characterise the pristine column state and to monitor changes in the columns during the test loading sequence. In some sense these white noise tests can be thought of as ambient-like responses to very small ground-borne

vibrations due to micro-quakes, traffic, and other natural sources. In the case of a large seismic event that may cause damage, there are normally many low amplitude aftershocks that will fill this role.

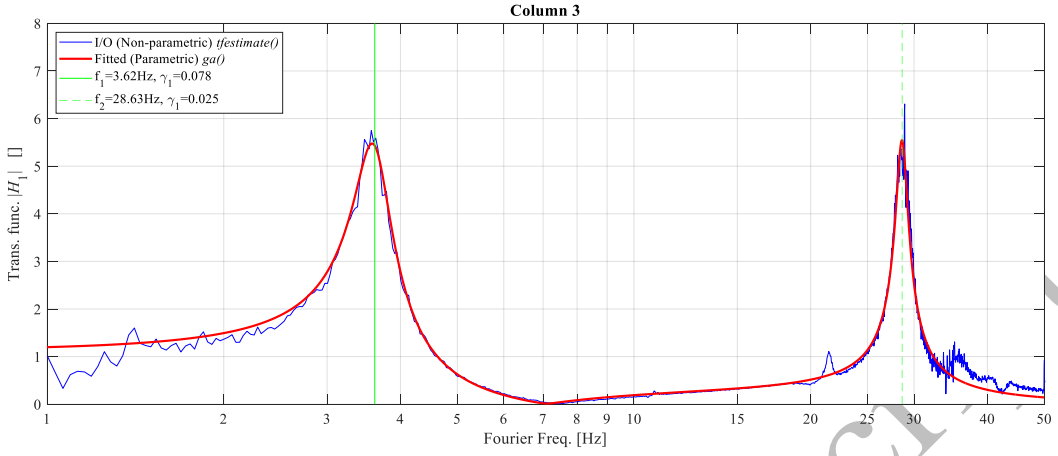

Figure 9, Transfer function estimates of physical RC column 3 using laboratory white noise test data, Ge et al. (2020a, b, c). Welch's algorithm (blue line) (a non-parametric estimate) and the system identification using a genetic algorithm (a parametric estimate) based on solving Eqn (10) (red line)

5.1 Multimodal linear system identification results

Figure 9 shows the results of extracting the linear kernel for the pristine column 3. The genetic algorithm is able to identify a very good fit using the theoretical equation (9) by solving the nonlinear optimisation problem defined in equation (10). This approach captures very well (with just 2 modes) the first (3.62Hz) and second mode (28.63Hz) resonances, and the anti-resonance (7.1Hz). The red lines are the fitted results (genetic algorithm, Goldberg (1989), Conn AR et al, (1991, 1997)) and blue lines are the classical, non-parametric, estimate of the transfer function using input and output (Vold et al (1984)). Note, by using this non-parametric estimate of the transfer function alone (without a genetic algorithm or some such inverse system ID algorithm) we are unable to obtain directly or very precisely estimates of the damping ratios which are very important.

Table 1 displays the initial fitted estimates of system parameters (assuming a 2-dof model) for all 4 RC test columns. Results indicate that the overall goodness of fit of equation (9) is excellent in the frequency range 1 to 50Hz.

Table 1, Results from a genetic algorithm 2-mode system identification of RC columns

RC Column	Fit parameters								
	$\omega_1/2\pi$ [Hz]	γ_1 [ ]	ρ_{11} [ ]	ρ_{12} [ ]	$\omega_2/2\pi$ [Hz]	γ_2 [ ]	ρ_{21} [ ]	ρ_{22} [ ]	r^2 [ ]
1	2.87	0.0690	267.4	-0.6437	27.39	0.0340	8152	-3.888	0.961
2	3.29	0.0781	383.0	-0.0516	27.62	0.0184	8374	-2.671	0.913
3	3.62	0.0782	438.7	-0.9443	28.63	0.0253	9045	-4.142	0.946
4	3.65	0.0774	423.3	-0.6708	29.75	0.0207	8649	-2.966	0.948

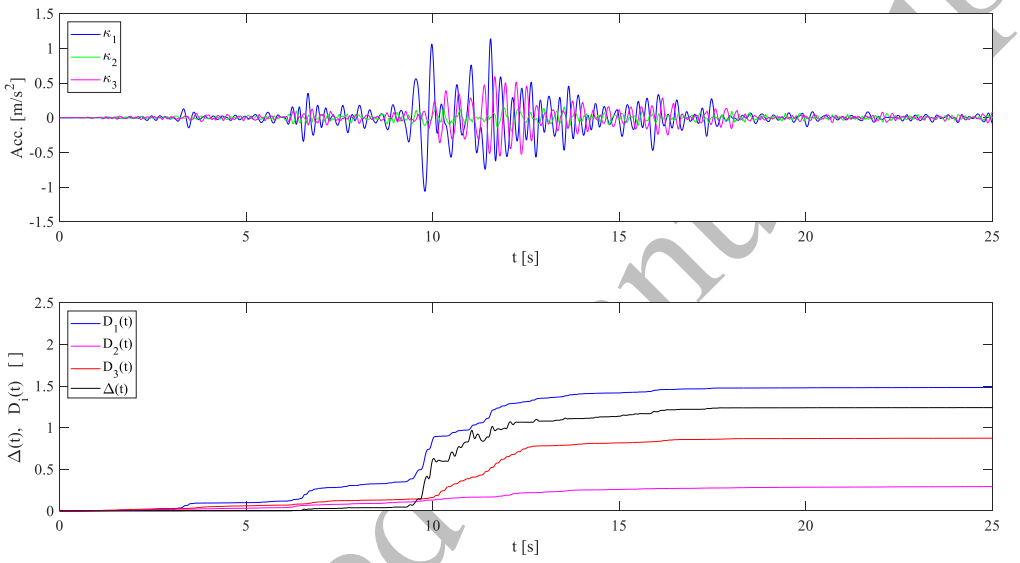

Figure 10, Example of RC Column 4 response data processing with Volterra series (method A) and hysteretic energy approach (method A/D). (top) extracted acceleration Volterra kernel series (bottom) cumulative damage measures $D_i(t)$ (method A) and $\Delta(t)$ (method A/D)

5.2 Applying Volterra series to experimental RC columns response acceleration data.

The four RC columns (Ge et al, 2020a,b,c) had differing reinforcement detailing and were subjected to different ground excitations in the laboratory experiments. Initially, a scaled PGA at 25% of the earthquakes recorded PGA in the field was used. We use response data to assess the extent of damage (which should be small) via Volterra series extraction $D_i(t)$ (equation (29), method A) and normalised hysteretic energy dissipation $\Delta(t)$ (using equation (39), method A/D). Note that equation (39) is based on a single dof idealisation and Figure 9 highlights that this system has at least two significant linear modes. Hence, to focus solely on the first resonance, we high-cut, zero phase, filter all recorded accelerations and displacements at 10Hz. Figure 10 displays results for Column 4 as an example. The extracted cumulative norms of the Volterra series $D_i(t)$ (method A) are compared with $\Delta(t)$ (method A/D). Note that the time-located initiation of minor damage (cracking) at around t=10s is identified by the cubic Volterra series $D_3(t)$. Results for all RC column tests are presented alongside the empirical

fit and prediction bounds of the Bouc-Wen model in Figure 11(a). All four column test results lie well within the 95% prediction bounds. This small sample of test data is consistent with the results of the Bouc-Wen model simulations. Results in Figure 11(b) indicate that all columns lie in the range $0.3 < D_{3,n} < 1$. This suggests that all columns have well distributed flexurally induced tension cracks in the concrete (which is the case). Column 2 has a predicted low probability (2%) of significant cracking (due to the ductility exceeding 1) while columns 1, 3 and 4 have a 65%, 89% and 93% predicted probability respectively of significant cracking (due to the ductility exceeding 1).

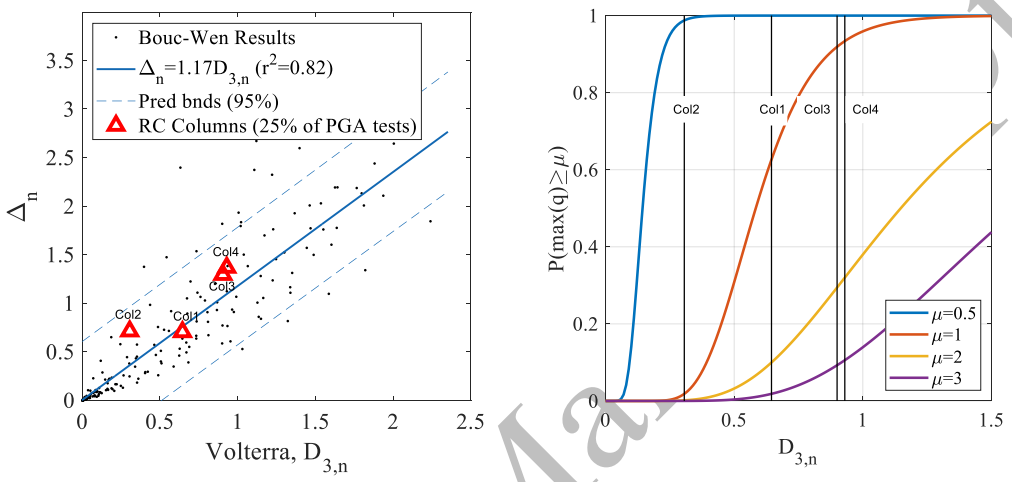

(a) (b)

Figure 11, Comparison of using Bouc-Wen predictions with extracted values from the four experimental RC columns data (Ge et al 2020a,b,c) (a) Cubic Volterra series norm (method A) vs hysteretic damage estimate (method A/D) (b) column data plotted on estimated fragility curves

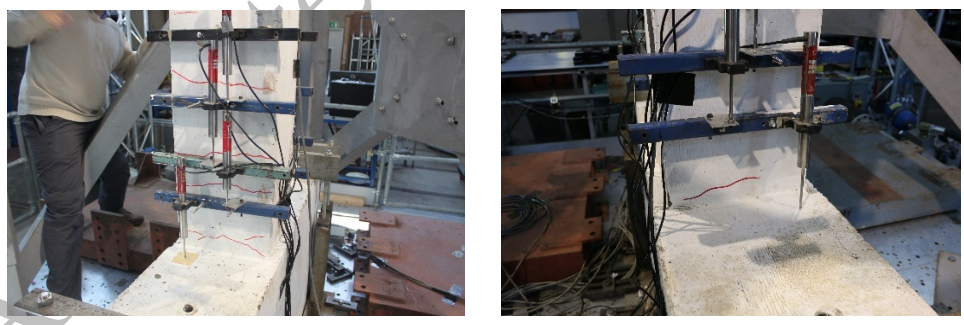

(a) (b)

Figure 12, Visual damage after 25% of PGA earthquake (Ge et al 2020a,b,c) (a) Column 1 (b) Column 2. Red lines on photos as visually identified large crack in cover concrete. Column 1 has more cracks (damage) than Column 2.

Results from Volterra series inverse system identification analysis Figure 11 suggest that it is probable that column 1 is more damaged than column 2. Visual inspection shown in the photos of Figure 12 agree with this acceleration only inference: column 1 was factually more damaged than column 2. Columns 3 and 4 showed more damage as indicated by both the Volterra series (method A) and force-deflection data (method A-D) although we do not have photographic confirmation for these columns.

Conclusions

The key research question of this paper was: can the level of seismically induced damage in a structure be determined from acceleration data alone? Results suggest an approach based on a Volterra series expansion based on multinomial combinations of a wavelet basis of the ground accelerations can be effective in a probabilistic sense in predicting the likely levels of damage.

In a heuristic numerical case of a bridge pier modelled by a nonlinear Bouc-Wen system the Volterra series/genetic algorithm approach can determine when, in time, damage starts to occur and estimate its likely (in a probabilistic sense) magnitude. This was demonstrated for a data set of 20 earthquakes with a large range of different scaling PGA amplitudes with the bridge pier modelled exhibiting a complete range of damage levels from low to high.

Physical experimental RC column tests are used to assess the utility of the numerical procedure in a practical setting. Damage estimates using method A/D are very similar (statistically) to the results using method A. Results from the probabilistic estimate of damage (method A), based on Volterra series/genetic algorithm approach, are consistent with the post-earthquake visual inspection of cracks in the columns.

The Volterra series/Genetic algorithm damage measure (method A, that uses only recorded structural acceleration responses) and the hysteretic energy dissipation damage measure (method A/D, that uses recorded Structural Acceleration and Displacement responses) are compared for this nonlinear bridge pier model. Results indicate that both methods are of similar accuracy (statistically), and this suggests that only accelerometers are necessary.

Thus, we present a case in favour of using accelerometers alone and a method for an effective rapid damage assessment of wide-scale, important infrastructure artefacts without the need for the extra expense of mounting parallel relative displacement transducer systems.

729

730

731

732

733 # References

734 Afsar Dizaj, E., & Kashani, M. M. (2020). "Numerical investigation of the influence of cross-sectional
735 shape and corrosion damage on failure mechanisms of RC bridge piers under earthquake loading".
736 *Bulletin of Earthquake Engineering*, 18, 4939-4961.

737 Ahlborn, T. M., Shuchman, R., Sutter, L. L., Brooks, C. N., Harris, D. K., Burns, J. W., Endsley, K. A.,
738 Evans, D. C., Vaghefi, K., & Oats, R. C. (2010). "The State-of-the-Practice of Modern Structural
739 Health Monitoring for Bridges: A Comprehensive Review". *Transportation Research Board, USA*

740 Alexander NA, Chanerley AA, Crewe AJ & Bhattacharya S, (2014) "Obtaining spectrum matching
741 time-series using a Re-weighted Volterra Series Algorithm (RVSA)", *Bulletin of the Seismological*
742 *Society of America*, 106(4)

743 Alipour, A., Shafei, B., & Shinozuka, M. (2011). "Performance evaluation of deteriorating highway
744 bridges located in high seismic areas." *Journal of Bridge Engineering*, 16(5), 597–611.

745 Aschheim, M., Moehle, J. P., & Werner, S. D. (1993). "Deformability of concrete columns". *Oakland,*
746 *Calif, Dames & Moore.*

747 Bedon, C., Bergamo, E., Izzi, M., & Noè, S. (2018). "Prototyping and validation of MEMS
748 accelerometers for structural health monitoring—The case study of the Pietratagliata cable-stayed
749 bridge". *Journal of Sensor and Actuator Networks*, 7(3), 30.

750 Bhattacharya S, Krishna M, Lombardi D, Crewe AJ & Alexander NA, (2012) "Economic MEMS based
751 3-axis water proof accelerometer for dynamic geo-engineering applications", *Soil Dynamics and*
752 *Earthquake Engineering*, pp. 111-118

753 Billings, S. A., Chen, A., & Korenberg, M. J. (1989). "Identification of MIMO nonlinear systems using
754 a forward-regression orthogonal algorithm". *International Journal of Control*, 49, 2157–2189

755 Byrd, R. H., Gilbert J. C., and Nocedal J., (2000) "A Trust Region Method Based on Interior Point
756 Techniques for Nonlinear Programming." *Mathematical Programming*, Vol 89, No. 1, pp. 149–185.

757 Byrd, R. H., Hribar M. E., and Nocedal J., (1999) "An Interior Point Algorithm for Large-Scale
758 Nonlinear Programming." *SIAM Journal on Optimization*, Vol 9, No. 4, pp. 877–900.

759 Caltrans. (2013). "Seismic Design Criteria" Version 1.7.

760 CEN.EN. (2010). "Eurocode 8 - Design provisions for earthquake resistance of structures - Part 2:
761 Bridges."

762 Ceylan, H., Gopalakrishnan, K., Kim, S., Taylor, P. C., Prokudin, M., & Buss, A. F. (2013). "Highway
763 infrastructure health monitoring using micro-electromechanical sensors and systems (MEMS)".
764 *Journal of Civil Engineering and Management*, 19(sup1), S188-S201.

765 Chanerley AA, Alexander NA, "Obtaining Estimates of Low frequency 'fling', instrument tilts and
766 displacement time-series using wavelet decomposition", 8(2), pp 231–255, *Bulletin of Earthquake*
767 *Engineering*, 2009.

Chanerley AA, Alexander NA, J. Berrill, H. Avery, B. Halldorsson & R. Sigbjornsson, (2013) "Concerning baseline errors in the form of acceleration transients when recovering displacements from strong motion records using the undecimated wavelet transform", *Bulletin of the Seismological Society of America*, 103(1) pp. 283-295

Charalampakis A, Koumousis V (2006). "Parameter estimation of Bouc-Wen hysteretic systems using a sawtooth genetic algorithm". *Proceedings of the 5th International Conference on Engineering Computational Technology, Civil-Comp Press.*

Cheng CM, Peng ZK, Dong XJ, Zhang WM, Meng G. (2015) "A novel damage detection approach by using Volterra kernel functions based analysis". *Journal of the Franklin Institute*. 352(8):3098-112.

Choe, D. E., Gardoni, P., Rosowsky, D., & Haukaas, T. (2008). "Probabilistic capacity models and seismic fragility estimates for RC columns subject to corrosion". *Reliability Engineering & System Safety*, 93(3), 383–393.

Chopra AK, (2019), "Dynamics of Structures, 5th Edition", *Pearson Ed. Ltd*.

Coifman, R.R., Donoho, D.L. (1995), "Translation invariant de-noising," *Lecture Notes in Statistics*, 103, pp. 125–150.

Conn A.R., Gould N. I. M., & Toint Ph. L., (1991) "A Globally Convergent Augmented Lagrangian Algorithm for Optimization with General Constraints and Simple Bounds", *SIAM Journal on Numerical Analysis*, Volume 28, Number 2, pages 545–572,

Conn A.R., Gould N. I. M., & Toint Ph. L., (1997) "A Globally Convergent Augmented Lagrangian Barrier Algorithm for Optimization with General Inequality Constraints and Simple Bounds", *Mathematics of Computation*, Volume 66, Number 217, pages 261–288

Cremen, G., & Baker, J. W. (2018). Quantifying the benefits of building instruments to FEMA P-58 rapid post-earthquake damage and loss predictions. *Engineering Structures*, 176, 243-253.

de Paula, N., Marques, F. D., & Silva, W. A. (2019). "Volterra Kernels Assessment via Time-Delay Neural Networks for Nonlinear Unsteady Aerodynamic Loading Identification". *AIAA journal. American Institute of Aeronautics and Astronautics*, 57(4), 1725–1735.

Dhakal, R. P., & Maekawa, K. (2002). Reinforcement Stability and Fracture of Cover Concrete in Reinforced Concrete Members. *Journal of Structural Engineering*, 128(10), 1253–1262.

Dizaj, E. A., Madandoust, R., & Kashani, M. M. (2018). "Exploring the impact of chloride-induced corrosion on seismic damage limit states and residual capacity of reinforced concrete structures." *Structure and Infrastructure Engineering*, 14(6), 714–729.

El-Bahy, A., Kunnath, S. K., Stone, W. C., & Taylor, A. W. (1999). "Cumulative seismic damage of circular bridge columns: benchmark and low-cycle fatigue tests". *ACI Structural Journal*, 96(4), 633–641.

Fa-Long, L. (2011). "Digital Front-End in Wireless Communications and Broadcasting", *Cambridge University Press, United Kingdom.*

FEMA-P695. (2009). "Quantification of building seismic performance factors".

Gallucci, L., Menna, C., Angrisani, L., Asprone, D., Moriello, R. S. L., Bonavolontà, F., & Fabbrocino, F. (2017). "An embedded wireless sensor network with wireless power transmission capability for the structural health monitoring of reinforced concrete structures". *Sensors*, 17(11), 2566.

Ge X, Alexander NA; Kashani MM, (2020a), "Rapid post-earthquake damage assessment of RC bridge piers using time-frequency analysis", *Structure and Infrastructure Engineering* ,

Ge X, Alexander NA, Dietz M, Kashani MM, (2020b) "Nonlinear dynamic behaviour of severely corroded reinforced concrete columns: shaking table study", *Bulletin of Earthquake Engineering*,

Ge X, (2020c) "Seismic Performance of Corroded RC Bridge Piers, A Large-Scale Shaking Table Study" PhD Thesis, University of Bristol

Ghosh, J., & Padgett, J. E. (2010). "Aging considerations in the development of time-dependent seismic fragility curves." *Journal of Structural Engineering*, 136(12), 1497–1511.

German, S., Brilakis, I., & DesRoches, R. (2012). "Rapid entropy-based detection and properties measurement of concrete spalling with machine vision for post-earthquake safety assessments". *Advanced Engineering Informatics*, 26(4), 846-858.

Giri, P., & Kharkovsky, S. (2016). "Detection of surface crack in concrete using measurement technique with laser displacement sensor". *IEEE Transactions on Instrumentation and Measurement*, 65(8), 1951-1953.

Giri, P., Kharkovsky, S., & Samali, B. (2017). "Inspection of metal and concrete specimens using imaging system with laser displacement sensor". *Electronics*, 6(2), 36.

Goldberg, David E., "Genetic Algorithms in Search, Optimization & Machine Learning", *Addison-Wesley*, 1989.

Goulet, J. A., Michel, C., & Kiureghian, A. D. (2015). "Data-driven post-earthquake rapid structural safety assessment". *Earthquake Engineering & Structural Dynamics*, 44(4), 549-562.

Kashani, MM., Ge, X., Dietz, MS. Crewe, AJ. Alexander, NA. (2019) "Significance of non-stationary characteristics of ground-motion on structural damage: shaking table study". *Bulletin of Earthquake Engineering* **17,** 4885–4907

Kashani, M. M., Maddocks, J., & Dizaj, E. A. (2019). "Residual Capacity of Corroded Reinforced Concrete Bridge Components: State-of-the-Art Review". *Journal of Bridge Engineering*, 24(7), 03119001.

Kim, T. H., Lee, K. M., Chung, Y. S., & Shin, H. M. (2005). "Seismic damage assessment of reinforced concrete bridge columns." *Engineering Structures*, 27(4), 576–592.

Kijewski-Correa, T. (2005). "GPS: a new tool for structural displacement measurements". *APT Bulletin*, 36(1), 13–18

Lang Zi-Quang, Billings SA. (1997) "Output frequencies of nonlinear systems". *International Journal of Control*. 67(5):713-30.

Lehman, D., Moehle, J., Mahin, S., Calderone, A., & Henry, L. (2004). "Experimental Evaluation of the Seismic Performance of Reinforced Concrete Bridge Columns". *Journal of Structural Engineering*, 130(6), 869–879

Libera, A. D., Carli, R., & Gianluigi Pillonetto, G. (2021). Kernel-based methods for Volterra series identification, Automatica, Volume 129

Lind, I., & Ljung, L. (2005). "Regressor selection with the analysis of variance method". *Automatica*, 41(4), 693–700.

Lynch, J. P. (2007). "An overview of wireless structural health monitoring for civil structures". *Philosophical Transactions of the Royal Society A: Mathematical, Physical and Engineering Sciences*, 365(1851), 345-372.

Meibodi AA, Alexander NA, (2020) 'Exploring a generalized nonlinear multi-span bridge system subject to multi-support excitation using a Bouc-Wen hysteretic model', *Soil Dynamics and Earthquake Engineering*,

Misiti M, Misiti Y, Oppenheim G, Poggi, JM, (2020), "Wavelet toolbox, Getting started Guide, Matlab" *Matlab*

Nason, G.P., Silverman B.W. (1995), "The stationary wavelet transform and some statistical applications," *Lecture Notes in Statistics*, 103, pp. 281–299.

Noda, D, Seki K, Iwasaki M, (2016) "Composite filter design and application to piezo-driven stage systems," *2016 IEEE 14th International Workshop on Advanced Motion Control (AMC)*, pp. 227-232

PEER (2010). "Pacific Earthquake Engineering Research Center (PEER) ground motion database." http://peer.berkeley.edu/peer_ground_motion_database/.

Pesquet, J.C., Krim H., Carfatan H., (1996), "Time-invariant orthonormal wavelet representations," *IEEE Trans. Sign. Proc*., vol. 44, 8, pp. 1964–1970.

Powers E. J., Ritz C. P., An C. K., Kim S. B., Miksad R. W. and Nam S. W., (1989) "Applications Of Digital Polyspectral Analysis To Nonlinear Systems Modeling And Nonlinear Wave Phenomena," *Workshop on Higher-Order Spectral Analysis*, pp. 73-77

Priestley, M. J. N. (2000). Performance based seismic design. *Bulletin of the New Zealand Society for Earthquake Engineering*, *33*(3), 325-346.

Priestley, M.J.N, Verma R, Xiao Y, (1994) "Seismic shear strength of reinforced concrete columns" *Journal of Structural Engineering*, ASCE, 120(8).

Rainieri, C., Fabbrocino, G., Manfredi, G., & Dolce, M. (2012). "Robust output-only modal identification and monitoring of buildings in the presence of dynamic interactions for rapid post-earthquake emergency management". *Engineering Structures*, 34, 436-446.

Rugh W.J., (1981) "Nonlinear System Theory: The Volterra/Wiener Approach". *Baltimore: The Johns Hopkins Press*,

Schölkopf, B., & Smola, A. J. (2001). "Adaptive computation and machine learning, Learning with kernels: Support vector machines, regularization, optimization, and beyond". *MIT Press*.

Song J, Der Kiureghian A. (2006), "Generalized Bouc–Wen model for highly asymmetric hysteresis". *J Eng Mech* 132:610–8.

Sheikh, S. A., & Khoury, S. S. (1993). "Confined concrete columns with stubs". *ACI Structural Journal*, 90(4), 414–431.

Schetzen, M. (1980). "The Volterra and Wiener Theories of Nonlinear Systems", *Wiley, New York*

Tobbi, H., Farghaly, A. S., & Benmokrane, B. (2014). "Behavior of Concentrically Loaded Fiber-Reinforced Polymer Reinforced Concrete Columns with Varying Reinforcement Types and Ratios." *ACI Structural Journal*, 111(2), 375–386

Tawfiq, I., Vinh, T. (2004) "Nonlinear Behaviour of Structures Using the Volterra Series—Signal Processing and Testing Methods". *Nonlinear Dynamics* 37, 129-149

Vamvatsikos, D., & Cornell, C. A. (2002). £Incremental dynamic analysis". *Earthquake engineering & Structural dynamics*, 31(3), 491-514.

Vicente, M. A., Gonzalez, D. C., Minguez, J., & Schumacher, T. (2018). "A novel laser and video-based displacement transducer to monitor bridge deflections". *Sensors*, 18(4), 970.

Vold, H., Crowley J., and Rocklin T.G, (1984) "New Ways of Estimating Frequency Response Functions." *Sound and Vibration*. Vol. 18, November 1984, pp. 34–38.

Volterra, Vito (1887). "Sopra le funzioni che dipendono da altre funzioni. III. Italy": R. Accademia dei Lincei. pp. 97–105.

Yashinsky, M., Ostrom, T. (2000) "Caltrans New Seismic Design Criteria for Bridges" *Earthquake Spectra*, 16 (1), pp. 285-307.

Appendix A: Derivation of linear multimodal transfer function

A generalised 2D linear elastic *n*-dof system subject to base excitation (earthquakes) takes the following form

$$\mathbf{M}\ddot{\mathbf{x}} + \mathbf{C}\dot{\mathbf{x}} + \mathbf{K}\mathbf{x} = \mathbf{C}\mathbf{1}\dot{x}_g + \mathbf{K}\mathbf{1}x_g \tag{40}$$

Where $\mathbf{M},\mathbf{C},\mathbf{K}$ are mass, orthogonal damping, and stiffness matrices, $\mathbf{x}$ are the dofs (defined with respect to a fixed coordinate frame which are often termed 'total displacements'), $\mathbf{1}$ is a column vector of ones, and x_g is the ground displacement time-series (the earthquake). By obtaining the matrix of eigenvectors $\mathbf{\Phi}$ of dynamic matrix $\mathbf{M}^{-1}\mathbf{K}$ we can introduce normal (modal) coordinates $\mathbf{x} = \mathbf{\Phi}\mathbf{q}$ and hence transform eqn (40) into an uncoupled form for the *i*th mode as follows,

$$\ddot{q}_i + 2\gamma_i\omega_i\dot{q}_i + \omega_i^2 q_i = p_{i1}x_g + p_{i2}\dot{x}_g \tag{41}$$

where

$$2\gamma_i\omega_i = \frac{\boldsymbol{\phi}_i^T\mathbf{C}\boldsymbol{\phi}_i}{\boldsymbol{\phi}_i^T\mathbf{M}\boldsymbol{\phi}_i}, \quad \omega_i^2 = \frac{\boldsymbol{\phi}_i^T\mathbf{K}\boldsymbol{\phi}_i}{\boldsymbol{\phi}_i^T\mathbf{M}\boldsymbol{\phi}_i}, \quad p_{i1} = \frac{\boldsymbol{\phi}_i^T\mathbf{K}\mathbf{1}}{\boldsymbol{\phi}_i^T\mathbf{M}\boldsymbol{\phi}_i}, \quad p_{i2} = \frac{\boldsymbol{\phi}_i^T\mathbf{C}\mathbf{1}}{\boldsymbol{\phi}_i^T\mathbf{M}\boldsymbol{\phi}_i} \tag{42}$$

By taking the Fourier transform of sdof (single modal) equation (41) we convert this differential equation into a algebraic one, as follows

$$\ddot{q}_i(\omega) = \frac{(p_{i1} + \mathbf{i}\omega p_{i2})}{\left(\omega^2 - \omega_i^2 + \mathbf{i}2\gamma_i\omega_i\omega\right)}\ddot{x}_g(\omega) \tag{43}$$

Where $q_i(\omega)$ and $x_g(\omega)$ are the Fourier transforms of $q_i(t)$ and $x_g(t)$ respectively, and ω the Fourier frequency. Thus, the total acceleration responses are the sum of modal response $\ddot{\mathbf{x}}(\omega) = \mathbf{\Phi}\ddot{\mathbf{q}}(\omega)$ hence

$$\ddot{\mathbf{x}}(\omega) = \left\{\sum_{i=1}^{n} \frac{\boldsymbol{\phi}_i(p_{i1} + \mathbf{i}\omega p_{i2})}{\left(\omega^2 - \omega_i^2 + \mathbf{i}2\gamma_i\omega_i\omega\right)}\right\}\ddot{x}_g(\omega) \tag{44}$$

And hence the *jth* dof/row in $\ddot{\mathbf{x}}(\omega)$ takes the form,

$$\ddot{x}_j(\omega) = \left\{\sum_{i=1}^{n} \frac{\phi_{ij}p_{i1} + \mathbf{i}\omega\phi_{ij}p_{i2}}{\omega^2 - \omega_i^2 + \mathbf{i}2\gamma_i\omega_i\omega}\right\}\ddot{x}_g(\omega) = \left\{\sum_{i=1}^{n} \frac{\rho_{i1} + \mathbf{i}\omega\rho_{i2}}{\omega_i^2 - \omega^2 + \mathbf{i}2\gamma_i\omega_i\,\omega}\right\}\ddot{x}_g(\omega) \tag{45}$$

where

$$\rho_{i1} = \phi_{ij}p_{i1}, \quad \rho_{i2} = \phi_{ij}p_{i2} \tag{46}$$

Appendix B: Database of ground motions employed.

Twenty accelerograms, were selected from the PEER strong motion database. The records are selected so that their geometric mean is a spectral match to the target spectrum. As a heuristic case an EC8 type I horizontal elastic spectrum of 0.35g, on soil class A, with 5% of critical damping was used. The additional stratified selection criteria are that the records should be from events of magnitude 6 to 7.5 and be from ground of shear wave velocity $V_s \geq 800\text{m/s}$. All records are low-cut zero-phase filtered at 0.25Hz.

Table 2, Scaled Records from PEER strong motion database

NGA Rec No.	Record No. in paper	Event	Year	Station	Mag
284	1, 2	Irpinia-Italy-01	1980	Auletta	6.9
285	3, 4	Irpinia-Italy-01	1980	Bagnoli Irpinio	6.9
292	5, 6	Irpinia-Italy-01	1980	Sturno	6.9
296	7, 8	Irpinia-Italy-02	1980	Bagnoli Irpinio	6.2
297	9, 10	Irpinia-Italy-02	1980	Bisaccia	6.2
303	11, 12	Irpinia-Italy-02	1980	Sturno	6.2
455	13, 14	Morgan Hill	1984	Gilroy Array #1	6.19

765	15, 16	Loma Prieta	1989	Gilroy Array #1	6.93
957	17, 18	Northridge-01	1994	Burbank - Howard Rd.	6.69
1011	19, 20	Northridge-01	1994	LA - Wonderland Ave	6.69

935